RSC Advances

PAPER

View Article Online
View Journal | View Issue

Cite this: *RSC Adv.*, 2021, **11**, 36726

Cu assisted loading of Pt on CeO_2 as a carbon-free catalyst for methanol and oxygen reduction reaction†

Linchi Zou, *[ab] Jian Pan,[a] Feng Xu[c] and Junfeng Chen*[c]

The widely studied Pt/C catalyst for direct methanol fuel cells (DMFCs) suffers severe carbon corrosion under operation, which undermines the catalytic activity and durability. It is of great importance to develop a carbon-free support with co-catalytic functionality for improving both the activity and durability of Pt-based catalysts. The direct loading of Pt on the smooth surface of oxides may be difficult. Herein, the Cu assisted loading of Pt on CeO_2 is developed. Cu pre-coated CeO_2 was facilely synthesized and Pt was electrochemically deposited to fabricate the carbon-free $PtCu/CeO_2$ catalyst. The $PtCu/CeO_2$ catalyst has a mass activity up to 1.84 and 1.57 times higher than Pt/C towards methanol oxidation reaction (MOR) and oxygen reduction reaction (ORR), respectively. Better durability is also confirmed by chronoamperometry and accelerated degradation tests. The strategy in this work would be greatly helpful for developing an efficient carbon-free support of Pt-based catalysts for applications in DMFCs.

Received 18th July 2021
Accepted 6th November 2021

DOI: 10.1039/d1ra05501a

rsc.li/rsc-advances

1. Introduction

Methanol is a cheap fuel source but has higher energy density than hydrogen, making direct methanol fuel cells (DMFCs) a fascinating power source.[1,2] Pt or Pt based metallic nanoparticles (NPs) supported on carbon materials, including amorphous carbon, carbon nanotubes, graphene, *etc.*, are commonly used as efficient catalysts.[3–7] However, carbon suffers inevitable chemical and electrochemical oxidation due to the high moisture, high temperature, and high operation potentials.[8] The electrochemical corrosion occurs as followed:

$$C + H_2O \rightarrow CO + 2H^+ + 2e^- \quad (1)$$

Reaction (1) will be promoted in the presence of Pt based catalysts.[9] The carbon corrosion leads to the migration and aggregation of supporting metal NPs, which undermine the activity and durability of catalysts.

It is of great importance to develop the stable support for improving both activity and durability of catalyst. Exploring the carbon-free supports with co-catalytic functionality has proven to be an effective approach.[10–15] Many materials, such as $Ti_{0.7}Ru_{0.3}O_2$,[10] Magnéli phase Ti_8O_{15} nanowires,[13] and CeO_2,[15,16] were studied as potential catalyst supports of DMFC. Kozu and the co-workers reported a one-step electrochemical synthesis of Pt–CeO_2 composite thin films and received a 25 mV negative shift toward MOR.[15] Lin and the co-workers used poly(-vinylpyrrolidone) as template to synthesis porous CeO_2 as non-carbon support to load Pt.[16] Their as-synthesized catalysts showed nearly twice the activity of Pt/C toward MOR. However, the poor conductivity of such non-carbon materials emerges as a trouble. The surface of oxides is smooth and hence the interaction with Pt is so weak that Pt nanoparticles aggregate easily, leading to the poor activity and durability.

Herein, we explore a facile method, which can load Pt homogeneously on CeO_2 support *via* Cu pre-coating, to prepare a conductive, efficient, and stable carbon-free catalyst support for DMFC. CeO_2 is a widely studied oxide, which can promote the activity and stability of catalysts.[16,17] We found that Cu is able to coat on CeO_2 surface homogeneously, avoiding the aggregation. Moreover, it has been revealed that both Cu and CeO_2 can modify the Pt d-band centre to achieve better performance on methanol oxidation reaction (MOR) and oxygen reduction reaction (ORR).[16–19] We started with partially covering Cu NPs with CeO_2 *via* a one-pot synthesis method, and then electrodeposited Pt onto the uncovered Cu surface. As a result, the PtCu alloy NPs form and co-exist with CeO_2, such structure confines the metal NPs and prevents their migration (Scheme 1). Results show that the MOR, ORR, and durability of the as-prepared catalysts are improved compared to Pt/C.

[a]*College of Materials Science and Engineering, Fujian University of Technology, Fuzhou, 350118, China. E-mail: zoulinchi@fjut.edu.cn*

[b]*Fujian Provincial Key Laboratory of Advanced Materials Processing and Application, Fuzhou, 350118, China*

[c]*School of Materials Science and Engineering, Fuzhou University, Qishan Campus, Fuzhou, 350116, China. E-mail: chenjunfeng@fzu.edu.cn*

† Electronic supplementary information (ESI) available. See DOI: 10.1039/d1ra05501a

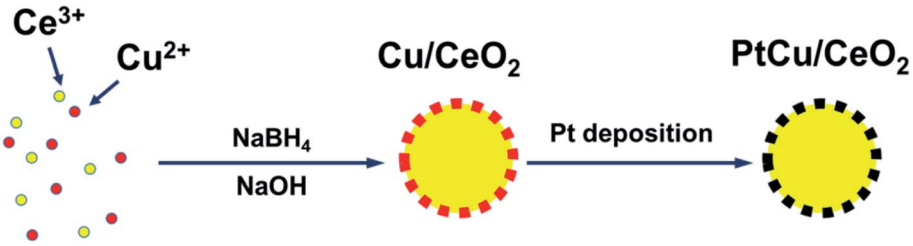

Scheme 1 The processes of synthesizing PtCu/CeO_2 catalysts.

2. Experimental

2.1 Materials

Chloroplatinic acid hexahydrate ($H_2PtCl_6 \cdot 6H_2O$), copper nitrate trihydrate [$Cu(NO_3)_2 \cdot 3H_2O$], cerium(III) nitrate hexahydrate [$Ce(NO_3)_3 \cdot 6H_2O$], sodium hydroxide (NaOH), sodium borohydride ($NaBH_4$), and glycerol were of analytical reagent (A.R.) grade and purchased from Sinopharm Chemical Reagent Co., Ltd. All chemicals were used as received. Deionized water (DI water, Millipore, 18.2 MΩ at 25 °C) were used in all processes.

2.2 Catalyst preparation

$Ce(NO_3)_3 \cdot 6H_2O$ and $Cu(NO_3)_2 \cdot 3H_2O$ at different molar ratio (Cu : Ce = 1 : 3, 1 : 2, 1 : 1, 2 : 1, and 3 : 1) were added into a three neck flask, then 100 mL of ethylene glycol (EG) were added, following the agitation at 80 °C overnight. 200 and 500 mg of NaOH and $NaBH_4$ were dissolved in 100 mL of DI water and slowly dropped into the flask. When the reaction finished, the Cu/CeO_2 composites were collected and rinsed with ethanol by centrifuging. The Cu/CeO_2 paste was freeze-dried.

For Pt electrodeposition, 6 mg of Cu/CeO_2 supports and 60 μL of Nafion solution (5% w/w, Dupont) were dispersed in 6 mL of isopropanol solution (isopropanol : DI water = 1 : 1). 10 μL of the resultant ink was pipetted onto the surface of glassy carbon electrode (GCE, $\phi = 5$ mm) and dried at room temperature. GCE was polished with Al_2O_3 (<50 nm) to a mirror-like surface before used. The electrode was immersed in the electrolyte containing 0.5 M H_2SO_4 and 3.86×10^{-3} M H_2PtCl_4, then subjected to the cyclic voltammetry (CV) scanning in the potential range of 0.0–1.2 V at 50 mV s^{-1} for 40 cycles. Pt wire and saturated calomel electrode (SCE) were used as counter and reference electrode, respectively. The catalysts with Cu : Ce ratios of 1 : 3, 1 : 2, 1 : 1, 2 : 1, and 3 : 1, were labelled as PtCu/CeO_2-13, PtCu/CeO_2-12, PtCu/CeO_2-11, PtCu/CeO_2-21, and PtCu/CeO_2-31, respectively.

2.3 Characterizations and electrochemical tests

X-ray diffraction (XRD) was performed on Ultima3 (D/teX) in the scanning 2θ range of 20–90° with Cu kα (λ = 0.15406 nm) as radiation source. The morphology of catalysts was obtained by transmission electron microscope (TECNAI G2F20, FEI). X-ray photoelectron spectroscopy (XPS) was performed on ESCALAB 250 (Thermo Scientific). The Pt loading was evaluated by inductively coupled plasma atomic emission spectrometry (ICP-MS, XSERIES 2, Thermo Fisher). CV was carried out in a three-electrode cell on CHI650D in the potential range of 0.0–1.2 V scanned at 50 mV s^{-1}. 0.5 M H_2SO_4 aqueous solution was used as electrolyte. Methanol electrooxidation was tested in 0.5 M H_2SO_4 and 1 M methanol electrolyte. To perform ORR, glassy carbon rotating-disk electrode was used as WE (RDE, $\phi = 5$ mm). Linear sweep voltammogram (LSV) measurements were

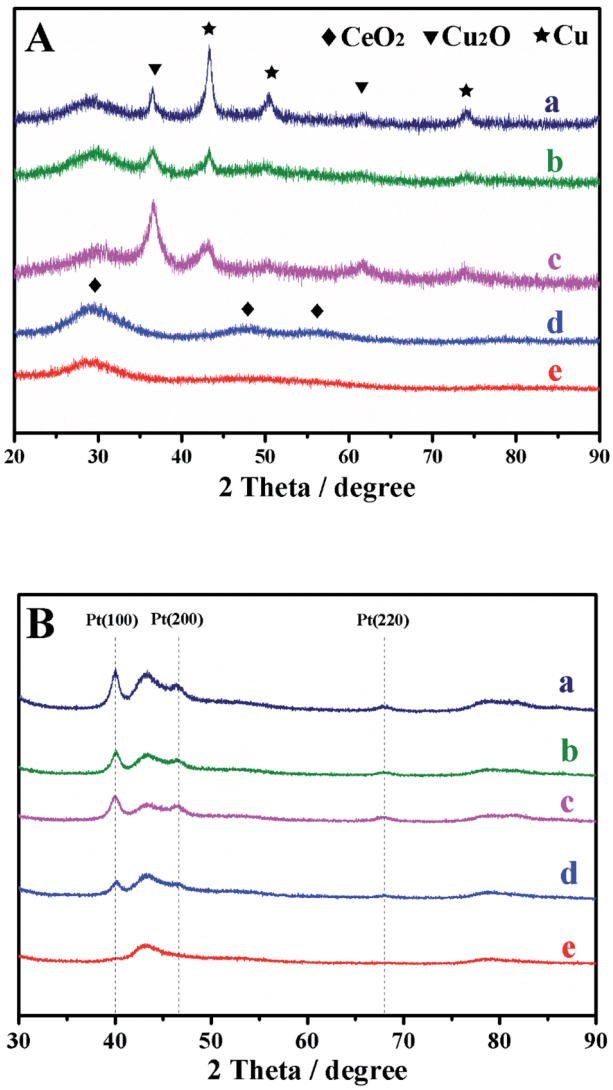

Fig. 1 XRD patterns of Cu–CeO_2 before (A) and after Pt deposition (B); (a), Cu–CeO_2-31; (b), Cu–CeO_2-21; (c), Cu–CeO_2-11; (d), Cu–CeO_2-12; (e), Cu–CeO_2-13.

performed in O_2-saturated 0.1 M $HClO_4$ solution at room temperature at the rotating speed of 1600 rpm and sweep rate of 10 mV s^{-1}. The kinetic current was calculated as followed:[20]

$$\frac{1}{I} = \frac{1}{I_k} + \frac{1}{I_d} \quad (2)$$

where I_k is the mass transport free kinetic current and I_d is the diffusion-limiting current. The values of I_d and I were chosen at 0.9 V and 0.2 V for calculation.

3. Results and discussion

3.1 Structure and morphology analysis

XRD was used to identify the structure of Cu pre-coated CeO_2 (Cu/CeO_2) (Fig. 1A). A broad peak in the range of 20–32° is ascribed to CeO_2(111) and (200) facets (JCPDS 34-0394). The peak at 47.5° is indexed to CeO_2(220). The vague diffraction signals indicate the very small particle size.[21] The characteristic peaks at 43.3°, 50.4°, and 74.1° belong to the metallic Cu(111), (200), and (220) facets (JCPDS 04-0836). The 2θ angles of Cu peaks are in very coincidence with JCPDS 04-0836, illustrating that CeO_2 did not affect the Cu crystal structure. We also observe the diffraction signals of Cu_2O which has the main peak at 36.4° accompanying with a weak one at 61.4°, ascribed to (111) and (220), respectively (JCPDS 05-0667). It is rational of the presence of Cu_2O because the lattice oxygen of CeO_2 could migrate to Cu surface in the condition of intimate contact.[16,17] As Cu dosage decreased, the Cu diffraction signals become fading, due to the lowering Cu contents in Cu/CeO_2. After Pt deposition, Pt signal emerges clearly expect on Cu/CeO_2-13 (Fig. 1B), due to the low metal content that not sufficient for XRD instrument to receive signal. Pt(100), Pt(200), and Pt(220) facets are identified at 40.0, 46.6, and 68.0°, which are all slightly higher than 2θ of JCPDS 04-0802. This indicates the PtCu alloy formation during Pt deposition.

The morphology and particle size of $PtCu/CeO_2$ with the Cu : Ce molar ratio of 2 : 1 were identified by TEM analysis (Fig. 2). TEM images of $PtCu/CeO_2$-12 and Pt/C were also offered (Fig. S1†). The $PtCu/CeO_2$ catalysts are the assembly of small nanoparticles (Fig. 2A and S1A†). The lattice with spacing value of 0.219 nm is commonly found. The value is between 0.226 nm of Pt(111) (JCPDS 04-0802) and 0.208 nm of Cu(111) (JCPDS 04-0836), which is a clear evidence of PtCu alloy.[22] The lattice belonging to CeO_2 could be barely found, but the EDS mapping reveals the homogeneous dispersion of Ce, Pt, and Cu elements (Fig. 2C–F). We propose that the PtCu alloy coats on CeO_2 surface.

The very intimate contact of CeO_2 and PtCu alloy can modify the electronic structure of Ce, Cu, and Pt elements, which is proven by XPS (Fig. 3). Ce 3d orbital is curve-fitted into satellite peaks belonging to Ce^{3+} (v_0, v', u_0, and u') and Ce^{4+} (v, v, v'', v''', u, u'', and u'''),[23,24] respectively (Fig. 3A). The peak u''' is

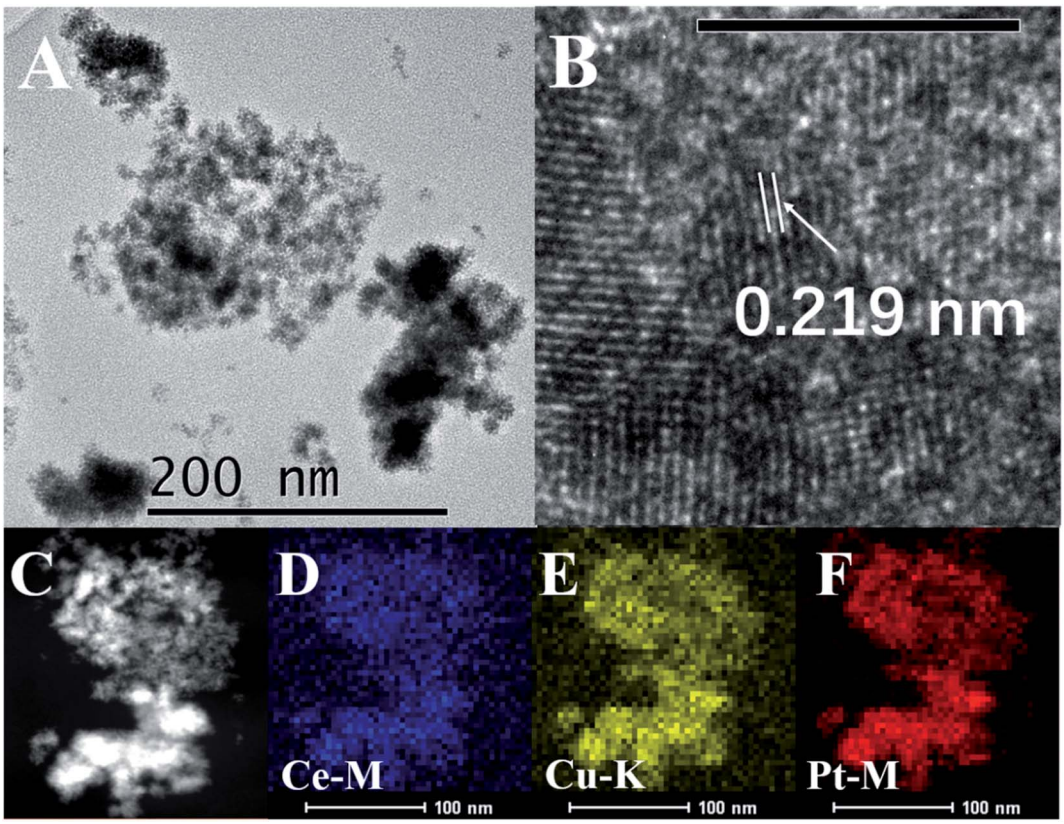

Fig. 2 TEM images of $PtCu/CeO_2$-21 catalyst (A). The scale bar in the image (B) is 5 nm. Image (C) shows the area chosen for elemental mapping, image (D, E, and F) show the mapping of Ce, Cu, and Pt, respectively.

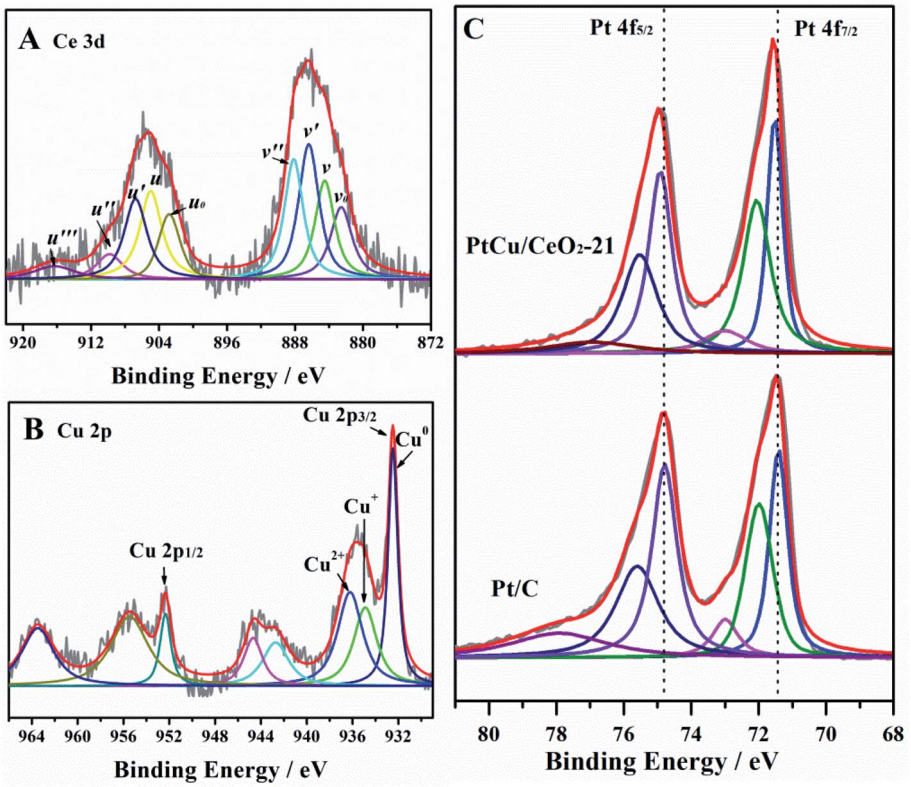

Fig. 3 The XPS analysis of Ce 3d (A), Cu 2p (B), and Pt-4f (C).

a characteristic signal of Ce^{4+}.[16] It is very weak here, demonstrating that the Ce^{4+} concentration in the CeO_2 NPs is relatively low, therefore, the concentration of oxygen vacancy is high.[24] The ratio $\Sigma Ce^{3+}/(\Sigma Ce^{3+} + \Sigma Ce^{4+})$ is commonly used to evaluate the Ce^{3+} fraction, *i.e.*, the oxygen vacancy concentration.[24] PtCu/CeO_2-21 has the ratio of 0.42. Cu 2p spectrum shows the co-existence of Cu, Cu^+ and Cu^{2+} (Fig. 3B). The peaks at 932.50 and 952.37 eV are attribute to Cu^0, the Cu^+ could be found close to Cu^0.[25] The shakeup satellite peaks at around 935, 944, 955, and 963 eV belong to Cu^{2+} species.[26,27] The intimate contact of CeO_2 and PtCu alloy NPs greatly facilitated the migration of lattice oxygen in the surface of CeO_2 to metal surface, and the electron transfer from PtCu to CeO_2, leading to the presence of high concentration of oxygen vacancy and metal oxide species.[16] Both CeO_2 and Cu can influence the Pt electronic structure, as a result, Pt 4f orbital shifts positively by 0.18 eV compared to that of Pt/C (Fig. 3C). The positive B.E. shift suggests that the d-band centre of Pt moves downwards, which will reduce the binding strength of adsorbents, leading to the enhancement of activity.[28,29]

3.2 Electrochemical activity and durability

The Cu-free Pt/CeO_2 shows no activity (Fig. S2†), hence, the discussion hereafter focuses on PtCu/CeO_2. Fig. S3† demonstrates the electrodeposition process during cyclic voltammetry (CV) cycles between 0.0–1.2 V *vs.* SHE at a scan rate of 50 mV s^{-1}. The peak at 0.34 V in the initial scans suggests the Cu dissolution from the Cu–CeO_2 support.[29,30] The Cu dissolution current fades as scanning goes on and dropped to undetectable level after five scans, indicating that Cu dissolution ceases. The peak at around 0.75 V is subject to the Pt reduction from the precursor. The Pt precursor ($PtCl_6^{2-}$) was reduced to Pt^0 following the probable reactions:[31,32]

$$PtCl_6^{2-} + 2e^- \rightarrow PtCl_4^{2-} + 2Cl^-,\ E^0 = 0.726\ \text{V SHE} \quad (3)$$

$$PtCl_4^{2-} + 2e^- \rightarrow Pt + 4Cl^-,\ E^0 = 0.758\ \text{V SHE} \quad (4)$$

$$PtCl_6^{2-} + 4e^- \rightarrow Pt + 6Cl^-,\ E^0 = 0.744\ \text{V SHE} \quad (5)$$

The anodic voltammetric responses at potentials higher than 0.95 V are associated with the formation of Pt surface oxide. On the cathodic scan, reduction peak at 0.7 V is related to the partial reduction of Pt oxide.[33] The hydrogen adsorption/desorption current in the potential range of 0–0.3 V arises as the deposition cycling goes on, which also illustrates the successful deposition of Pt. When the Pt electrodeposition was finished, the working electrodes were rinsed with plenty of DI water for electrochemical tests.

The CVs show familiar H ad/desorption (0–0.4 V) as well as Pt oxide formation (0.6–1.2 V) in 0.5 M H_2SO_4 (Fig. 4A). The onset potentials of Pt oxide formation of Pt/Cu–CeO_2 catalysts are more positive than Pt/C, indicating that Pt of PtCu/CeO_2 is more difficult to oxidize.[34] The Pt loading on the electrode surface was evaluated by atomic absorption spectrometry. The PtCu/CeO_2 catalysts show close Pt loading to Pt/C on the electrode surface (Fig. 4B). PtCu/CeO_2 catalysts with higher Cu content

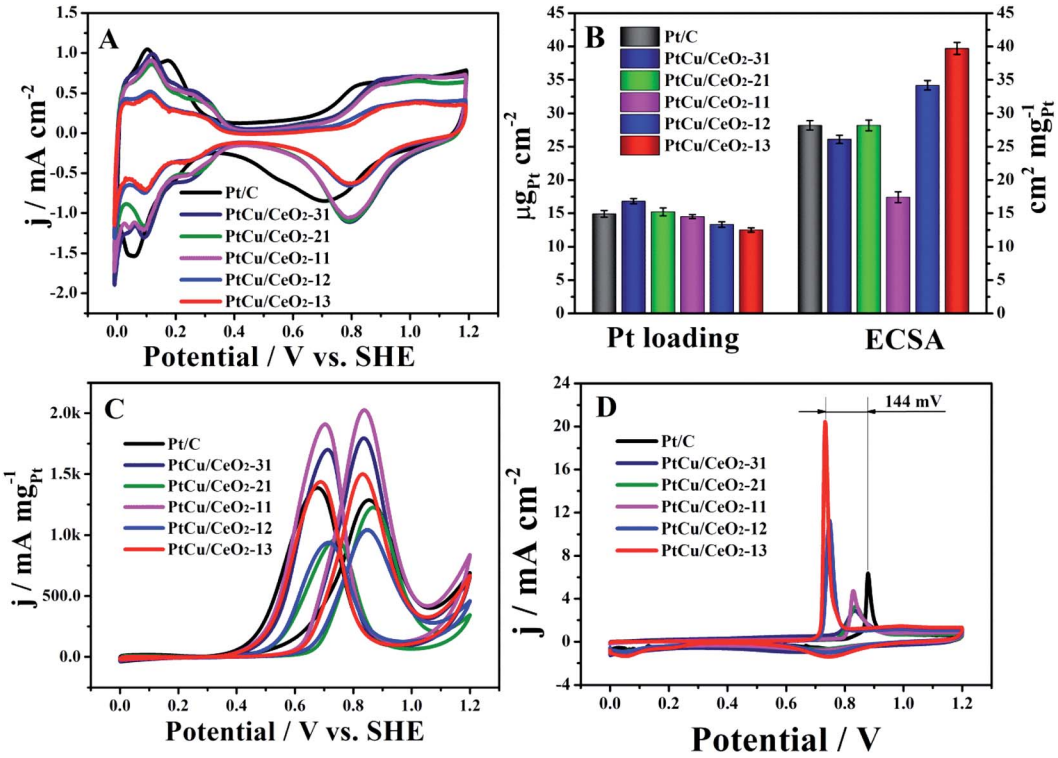

Fig. 4 (A): CVs of Pt/C and PtCu/CeO_2 catalysts in 0.5 M H_2SO_4; (B), Pt loading and ECSA values; (C), MOR mass activities of Pt/C and PtCu/CeO_2 catalysts in 0.5 M H_2SO_4 and 1 M CH_3OH; (D), CO stripping catalysts in 0.5 M H_2SO_4. The scan rate was 50 mV s^{-1}.

demonstrate higher Pt loading, illustrating that Pt is mainly deposited on the Cu surface. This agrees well with the TEM analysis. The electrochemical surface area (ECSA) was calculated by integrating the hydrogen desorption charge (Fig. 4B and Table 1). PtCu/CeO_2-13 and PtCu/CeO_2-12 shows higher ECSA than Pt/C, due to the lower Pt loading on the electrode. PtCu/CeO_2-31 and PtCu/CeO_2-21 have the close ECSA to Pt/C, while PtCu/CeO_2-11 has the lowest value. Fig. 4A and B show that the PtCu/CeO_2 catalysts have comparable electrochemical activity to Pt/C, evidencing that the presence of Cu efficiently ensures the conductivity. The very small particle size is also very beneficial for the catalytic activity.[35,36]

Fig. 4C shows the MOR activity of Pt/C and PtCu/CeO_2 catalysts. Both forward (I_f) and backward (I_b) peak currents of PtCu/CeO_2-13, PtCu/CeO_2-11 and PtCu/CeO_2-31 are higher than Pt/C, while PtCu/CeO_2-12 and PtCu/CeO_2-21 have the lower values (Table 1). The peak I_f is attributed to the partially oxidation of methanol to the carbonaceous species such as CO_{ads}, and the peak I_b comes from the removal of the incomplete oxidized carbonaceous species accumulated on Pt surface during the forward scan.[37,38] The ratio $I_f : I_b$ is used to evaluated the MOR performance of catalyst, *i.e.*, larger $I_f : I_b$ represents better poisoning tolerance and *vice versa*.[39] All PtCu/CeO_2 catalysts have higher $I_f : I_b$ than Pt/C, illustrating the better poison tolerance of PtCu/CeO_2. As shown in Table 1, PtCu/CeO_2-21 has the highest $I_f : I_b$ value of 1.27, which is 1.4 times higher than 0.92 of Pt/C. The CO stripping was performed for confirmation (Fig. 4D). During the first scans of all catalysts, signals related to hydrogen ad/desorption does not show, which is attributed to the CO coverage on Pt surface and no marginal for H adsorption. The sharp peaks in the potential range of 0.6–0.8 V belong to the CO oxidation.[40] The CO peak of Pt/C locates at 0.878 V,

Table 1 The electrochemical parameters of Pt/C and PtCu/CeO_2 catalysts

			MOR			ORR	
	Pt loading μg_{Pt} cm^{-2}	ECSA cm^{-2} mg_{Pt}^{-1}	I_f mA mg_{Pt}^{-1}	I_b mA mg_{Pt}^{-1}	$I_f : I_b$	MA mA mg_{Pt}^{-1}	SA mA cm_{Pt}^{-2}
Pt/C	14.9	28.2	1289.89	1388.92	0.92	127.96	4.54
PtCu/CeO_2-31	16.8	26.1	1804.01	1704.98	1.05	125.63	4.81
PtCu/CeO_2-21	15.2	28.2	1226.68	961.90	1.27	237.88	8.44
PtCu/CeO_2-11	14.5	17.1	2025.25	1914.63	1.06	153.67	8.68
PtCu/CeO_2-12	13.3	34.2	1040.91	942.23	1.11	177.52	5.19
PtCu/CeO_2-13	12.5	39.7	1507.62	1448.27	1.04	171.53	4.32

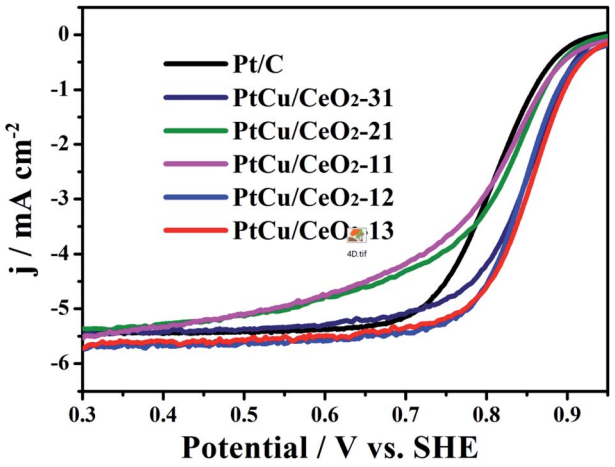

Fig. 5 The ORR curves obtained with on a glassy carbon rotating electrode disk in O_2-saturated 0.1 M $HClO_4$ solution at a sweep rate of 10 mV s^{-1}.

more positively than all the $PtCu/CeO_2$ catalysts, especially $PtCu/CeO_2$-12 (0.745 V) and $PtCu/CeO_2$-13 (0.734 V). One could find out that Cu is prone to enhance the MOR activity, due to the electronic effect,[41,42] because the compressive lattice resulting from alloy structure can weaken the binding of Pt surface atoms to adsorbed intermediates.[41]

The ORR polarization curves of Pt/C and $PtCu/CeO_2$ catalysts are shown in Fig. 5. The onset and half-wave potentials of $PtCu/CeO_2$ catalysts shift positively relative to Pt/C, implying the decrease in overpotential of ORR.[43] $PtCu/CeO_2$-21, $PtCu/CeO_2$-11, $PtCu/CeO_2$-12, and $PtCu/CeO_2$-13 exhibit the mass activity (MA) of 237.88, 153.67, 177.52, and 171.53 mA mg_{Pt}^{-1} on the basis of Pt mass at 0.9 V, which are 1.86, 1.20, 1.39, and 1.34 times of $MA_{Pt/C}$ (127.96 mA mg_{Pt}^{-1}) (Table 1). $PtCu/CeO_2$-31 exhibits MA value of 125.63 mA mg_{Pt}^{-1}, slightly lower than Pt/C. The surface-area-specific activity (SA) is calculated by dividing the mass activity by total ECSA on the electrode surface.[11] The SAs of $PtCu/CeO_2$-31, $PtCu/CeO_2$-21, $PtCu/CeO_2$-11, and $PtCu/CeO_2$-12 are 1.06, 1.86, 1.91, and 1.14 times higher than Pt/C (Table 1).

It is known that the binding energy is strongly related to the ad/desorption capability of reaction intermediates on the catalyst surface. The quantity oxygen vacancies can bind Pt more strongly due to the Pt-oxygen vacancy interaction.[44] Moreover, the oxygen vacancies decrease the energy barrier for lattice oxygen movement. The lattice oxygen at the Pt–CeO_2 interface is well accepted that key for promoting the methanol electrooxidation.[45] The positive shift of B.E. and the resulting downward-move of d-band centre of Pt 4f can decrease the B.E. of adsorbents, such as CO_{ads} and OH_{ads}, on the Pt surface, which facilitate the remove of adsorbents and promote the catalytic activity towards MOR and ORR.[34] Furthermore, the reduced Pt lattice constant which decrease the B.E. of OH_{ads} and the suppression of Pt oxide formation are also proposed to be responsible for the enhanced ORR of $PtCu/CeO_2$ catalysts, because OH_{ads} could inhibit the oxygen adsorption on Pt surface and Pt oxide has inherently lower ORR activity than bare Pt.[40,46]

The durability of catalyst is highly concerned and evaluated by chronoamperometry (CA) and accelerated degradation test (ADT). At the initial stage of CA measurements (Fig. 6A), $PtCu/CeO_2$-31, $PtCu/CeO_2$-21, $PtCu/CeO_2$-11, $PtCu/CeO_2$-12 and $PtCu/CeO_2$-13 catalysts exhibit the current densities of 16.45, 9.66, 18.81, 8.32, and 12.34 mA cm^{-2}, much higher than 2.74 mA cm^{-2} of Pt/C. During the CA operation, methanol was continuously oxidized and the intermediates (such as CO_{ads}) would accumulate on Pt surface,[47] leading to the catalyst poisoning and current decrease. Pt/Cu–CeO_2 exhibited a much slower decay of current density over time than Pt/C, due to a faster remove rate of intermediates on Pt surface and better CO tolerance.

It is interesting that after the 10 h continuous CA running, the I_f and I_b peak potentials of $PtCu/CeO_2$ move to lower potentials by upmost 30 mV, and the I_f:I_b values increase (Fig. S4 and S5†). The I_f:I_b values of $PtCu/CeO_2$-31, $PtCu/CeO_2$-21, $PtCu/CeO_2$-11, $PtCu/CeO_2$-12, and $PtCu/CeO_2$-13 catalysts are 1.23, 1.61, 1.28, 1.26, and 1.36, higher than their original values by 0.17, 0.34, 0.22, 0.15, and 0.20, respectively. Pt/C has no change in these features. The positive change of MOR activities of $PtCu/CeO_2$ catalysts indicates that the interaction

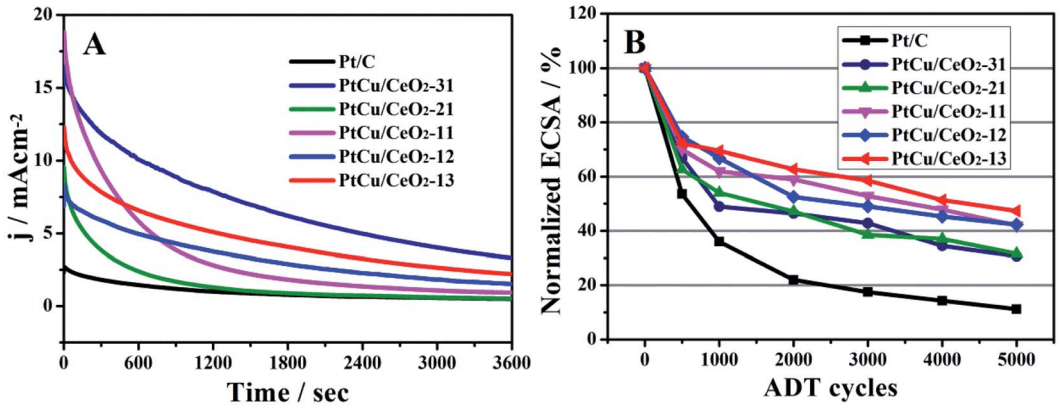

Fig. 6 (A), the chronoamperometry running at the constant potential of 0.6 V for 3600 s in 0.5 M H_2SO_4 and 1 M CH_3OH; (B), the relative change of ECSA obtained by ADT.

between Pt and Cu–CeO_2 support becomes stronger under operation.

ADT was carried out to further examine the durability of PtCu/CeO_2 catalysts (Fig. 6B and S6†). Pt suffers oxidation and dissolution in the potential range of 0.6–1.2 V by following reactions:[48,49]

$$Pt + H_2O \leftrightarrow PtO + 2H^+ + 2e^- \quad (6)$$

$$PtO + H_2O \leftrightarrow PtO_2 + 2H^+ + 2e^- \quad (7)$$

$$Pt \leftrightarrow Pt^{2+} + 2e^- \quad (8)$$

$$PtO + 2H^+ \leftrightarrow Pt^{2+} + H_2O \quad (9)$$

$$PtO_2 + 4H^+ \leftrightarrow Pt^{2+} + 2H_2O \quad (10)$$

Which lead to the loss of ECSA. After 5000 ADT scans, PtCu/CeO_2-31, PtCu/CeO_2-21, PtCu/CeO_2-11, PtCu/CeO_2-12 and PtCu/CeO_2-13 catalysts retain 31, 32, 42, 42, and 47% of initial ECSA. As a comparison, Pt/C has only 12% of initial ECSA left. Better durability is obtained with higher CeO_2 content. The oxygen vacancy has the effect of anchoring metal NPs, which could inhibit the migration and sintering, leading to an improved durability.[17,50]

4. Conclusion

The Cu pre-coated CeO_2 carbon-free support was facilely synthesized *via* a one-pot method and Pt was electrochemically deposited to fabricate the PtCu/CeO_2 catalyst. The PtCu/CeO_2 catalysts show higher activity toward methanol oxidation reaction and oxygen reduction reaction than Pt/C. The better durability is confirmed by chronoamperometry and accelerated degradation test. We find that Cu is preferential to the MOR enhancement, and CeO_2 leans to the improvement in ORR and durability. The downshift of Pt d-band centre of PtCu/CeO_2 catalysts, caused by the interaction between Pt and Cu–CeO_2 composite support, is responsible for the MOR, ORR, and durability enhancement. Besides, the compressive strain effect of Cu on Pt and the depression of Pt oxidation are beneficial to MOR and ORR, respectively; high concentration of oxygen vacancy of CeO_2 could strongly anchor metallic nanoparticles which inhibits the migration and sintering of Pt, leading to durability improvement.

Conflicts of interest

We declare that we do not have any commercial or associative interest that represents a conflict of interest in connection with the work submitted.

Acknowledgements

This work is financially supported by the National Natural Science Foundation of China (Grant No. 51901044 and 51871057), and Fujian Natural Science Foundation (2019J01227), and Natural Science Foundation for Youth Key Projects in College of Fujian (JZ160463), and Open research project of Fujian Provincial Key Laboratory of Advanced Materials Processing and Application (No. KF-C19003).

References

1 Z. M. Cui, H. Chen, M. T. Zhao, D. Marshall, Y. C. Yu, H. Abruña and F. J. DiSalvo, *J. Am. Chem. Soc.*, 2014, **136**, 10206–10209.
2 W. Y. Yuan, Y. Cheng, P. K. Sheng, C. M. Li and S. P. Jiang, *J. Mater. Chem. A*, 2015, **3**, 1961–1971.
3 J. Y. Cao, Y. Y. Du, M. M. Dong, Z. D. Chen and J. Xu, *J. Alloys Compd.*, 2018, **747**, 124–130.
4 Y. Y. Hu, J. Lu and H. Feng, *RSC Adv.*, 2021, **11**, 11918–11942.
5 F. J. García-Mateos, T. Cordero-Lanzac, R. Berenguer, E. Morallón, D. Cazorla-Amorós, J. Rodríguez-Mirasol and T. Cordero, *Appl. Catal., B*, 2017, **211**, 18–30.
6 H. Q. Song, M. S. Luo, X. P. Qiu and G. Z. Cao, *Electrochim. Acta*, 2016, **213**, 578–586.
7 T. C. Wu, M. Y. Gan, L. Ma, S. Wei, Q. L. Fu, Y. L. Yang, T. T. Li, F. Xie, W. Zhan and X. J. Zhong, *New J. Chem.*, 2021, **45**, 11035–11041.
8 X. X. Yuan, X. L. Ding, C. Y. Wang and Z. F. Ma, *Energy Environ. Sci.*, 2013, **6**, 1105–1124.
9 Z. K. Kou, K. Cheng, H. Wu, R. H Sun, B. B. Guo and S. C. Mu, *ACS Appl. Mater. Interfaces*, 2016, **8**, 3940–3947.
10 V. T. T. Ho, K. C. Pillai, H. L. Chou, C. J. Pan, J. Rick, W. N. Su, B. J. Hwang, J. F. Lee, H. S. Sheu and W. T. Chuang, *Energy Environ. Sci.*, 2011, **4**, 4194–4200.
11 T. Tamaki, H. Kuroki, S. Ogura, T. Fuchigami, Y. Kitamoto and T. Yamaguchi, *Energy Environ. Sci.*, 2015, **8**, 3545–3549.
12 N. R. Elezovic, V. R. Radmilovic and N. V. Krstajic, *RSC Adv.*, 2016, **6**, 6788.
13 P. K. Shen, C. Y. He, S. Y. Chang, X. D. Huang and Z. Q. Tian, *J. Mater. Chem. A*, 2015, **3**, 14416–14423.
14 K. E. Fritz, P. A. Beaucage, F. Matsuoka, U. Wiesner and J. Suntivich, *Chem. Commun.*, 2017, **53**, 7250–7253.
15 Y. Kozu, S. Kawashima and F. Kitamura, *J. Solid State Electrochem.*, 2013, **17**, 761–765.
16 B. F. Lin, Z. Lei, F. Xu, N. C. Cheng and S. C. Mu, *Electrochim. Acta*, 2018, **290**, 55–62.
17 F. Xu, D. Q. Wang, B. S. Sa, Y. Yu and S. C. Mu, *Int. J. Hydrogen Energy*, 2017, **42**, 13011–13019.
18 J. A. Wittkopf, J. Zheng and Y. S. Yan, *ACS Catal.*, 2014, **4**, 3145–3151.
19 M. L. Xiao, S. T. Li, X. Zhao, J. B. Zhu, M. Yin, C. P. Liu and W. Xing, *ChemCatChem*, 2014, **6**, 2825–2831.
20 I. S. Amiinu, Z. H. Pu, X. B. Liu, K. A. Owusu, H. G. R. Monestel, F. O. Boakye, H. N. Zhang and S. C. Mu, *Adv. Funct. Mater.*, 2017, **27**, 1702300.
21 Y. J. Cen, Q. W. Qin, R. D. Sisson and J. Y. Liang, *Electrochim. Acta*, 2017, **251**, 690–698.
22 Q. Dai, Y. Yang, Z. Zhao, A. Fisher, Z. P. Liu and D. J. Cheng, *Nanoscale*, 2017, **9**, 8945–8951.
23 L. Zhang and Y. Shen, *ChemElectroChem*, 2015, **2**, 887–895.
24 Z. P. Qu, F. L. Yu, X. D. Zhang, Y. Wang and J. S. Gao, *Chem. Eng. J*, 2013, **229**, 522–532.

25 K. Samson, M. Śliwa, R. P. Socha, K. Góra-Marek, D. Mucha, D. Rutkowska-Zbik, J.-F. Paul, M. Ruggiero-Mikołajczyk, R. Grabowski and J. Słoczyński, *ACS Catal.*, 2014, **4**, 3730–3741.
26 J. Y. Jin, H. Mei, H. M. Wu, S. F. Wang, Q. H. Xia and Y. Ding, *J. Alloys Compd.*, 2016, **689**, 174–181.
27 X. Y. Zhang, P. Gu, X. Y. Li and G. H. Zhang, *Chem. Eng. J.*, 2017, **322**, 129–139.
28 B. Y. Xia, H. B. Wu, N. Li, X. W. Lou and X. Wang, *Angew. Chem.*, 2015, **127**, 3868–3872.
29 M. L. Xiao, J. B. Zhu, J. J. Ge, C. P. Liu and W. Xing, *J. Power Sources*, 2015, **281**, 34–43.
30 M. Allemand, M. H. Martin, D. Reyter, L. Roué, D. Guay, C. Andrei and G. A. Botton, *Electrochim. Acta*, 2011, **56**, 7397–7403.
31 A. F. Ilkhchy, F. Nasirpouri, C. Bran and M. Vázquez, *J. Solid State Chem.*, 2016, **244**, 35–44.
32 H. Z. Yang, J. Zhang, K. Sun, S. Z. Zou and J. Y. Fang, *Angew. Chem., Int. Ed.*, 2010, **49**, 6848–6851.
33 X. W. Du, S. P. Luo, H. Y. Du, M. Tang, X. D. Huang and P. K. Shen, *J. Mater. Chem. A*, 2016, **4**, 1579–1585.
34 T. Ariyanto, A. M. Kern, B. J. M. Etzold and G. R. Zhang, *Electrochem. Commun.*, 2017, **82**, 12–15.
35 L. Zhang, K. D. Davis and X. L. Sun, *Energy Environ. Sci.*, 2019, **12**, 492–517.
36 N. C. Cheng, M. N. Banis, J. Liu, A. Riese, X. Li, R. Y. Li, S. Y. Ye, S. Knights and X. L. Sun, *Adv. Mater.*, 2015, **27**, 277–281.
37 K. Bhunia, S. Khilari and D. Pradhan, *ACS Sustainable Chem. Eng.*, 2018, **6**, 7769–7778.
38 K. Bhunia, S. Khilari and D. Pradhan, *Dalton Trans.*, 2017, **46**, 15558–15566.
39 G. L. Zhang, Z. Z. Yang, W. Zhang and Y. X. Wang, *J. Mater. Chem. A*, 2017, **5**, 1481–1487.
40 W. P. Xiao, J. Zhu, L. L. Han, S. F. Liu, J. Wang, Z. X. Wu, W. Lei, C. J. Xuan, H. L. L. Xin and D. L. Wang, *Nanoscale*, 2016, **8**, 14793–14802.
41 I. E. L. Stephens, A. S. Bondarenko, F. J. Perez-Alonso, F. Calle-Vallejo, L. Bech, T. P. Johansson, A. K. Jepsen, R. Frydendal, B. P. Knudsen, J. Rossmeisl and I. Chorkendorff, *J. Am. Chem. Soc.*, 2011, **133**, 5485–5491.
42 J. Y. Liu, G. R. Xu, B. C. Liu and J. Zhang, *Chem. Commun.*, 2017, **53**, 7457–7460.
43 S. Parwaiz, K. Bhunia, A. K. Das, M. M. Khan and D. Pradhan, *J. Phys. Chem. C*, 2017, **121**, 20165–20176.
44 H. Xu, A. L. Wang, Y. X. Tong and G. R. Li, *ACS Catal.*, 2016, **6**, 5198–5206.
45 G. L. Zhou, P. Li, Q. M. Ma, Z. X. Tian and Y. Liu, *Nano Lett.*, 2018, **18**, 1668–1677.
46 M. Y. Jing, L. H. Jiang, B. L. Yi and G. Q. Sun, *J. Electroanal. Chem.*, 2013, **688**, 172–179.
47 W. D. Zhang, Q. Z. Dong, H. Z. Lu, B. N. Hu, Y. Xie and G. Yu, *J. Alloys Compd.*, 2017, **727**, 475–483.
48 A. A. Topalov, S. Cherevko, A. R. Zeradjanin, J. C. Meier, I. Katsounaros and K. J. J. Mayrhofer, *Chem. Sci.*, 2014, **5**, 631–638.
49 M. Zhao, W. Y. Shi, B. B. Wu, W. M. Liu, J. G. Liu, D. M. Xin, Y. F. Yao, Z. J. Hou, P. W. Ming, J. Gu and Z. G. Zou, *Int. J. Hydrogen Energy*, 2014, **39**, 13725–13737.
50 S. W. Li, Y. Xu, Y. F. Chen, W. Z. Li, L. L. Lin, M. Z. Li, Y. C. Deng, X. P. Wang, B. H. Ge, C. Yang, S. Y. Yao, J. L. Xie, Y. W. Li, X. Liu and D. Ma, *Angew. Chem., Int. Ed.*, 2017, **56**, 1–6.